COLLINARUS: Collection of Image-derived Non-linear Attributes for Registration Using Splines

Jonathan Chappelow[a], B. Nicholas Bloch[b], Neil Rofsky[b], Elizabeth Genega[b], Robert Lenkinski[b], William DeWolf[b], Satish Viswanath[a], and Anant Madabhushi[a]

[a]Rutgers University, Department of Biomedical Engineering, Piscataway, NJ USA;
[b]Harvard University, Beth Israel Deacones Medical Center, Cambridge, MA USA

ABSTRACT

We present a new method for fully automatic non-rigid registration of multimodal imagery, including structural and functional data, that utilizes multiple texutral feature images to drive an automated spline based non-linear image registration procedure. Multimodal image registration is significantly more complicated than registration of images from the same modality or protocol on account of difficulty in quantifying similarity between different structural and functional information, and also due to possible physical deformations resulting from the data acquisition process. The COFEMI technique for feature ensemble selection and combination has been previously demonstrated to improve rigid registration performance over intensity-based MI for images of dissimilar modalities with visible intensity artifacts. Hence, we present here the natural extension of feature ensembles for driving automated non-rigid image registration in our new technique termed Collection of Image-derived Non-linear Attributes for Registration Using Splines (COLLINARUS). Qualitative and quantitative evaluation of the COLLINARUS scheme is performed on several sets of real multimodal prostate images and synthetic multiprotocol brain images. Multimodal (histology and MRI) prostate image registration is performed for 6 clinical data sets comprising a total of 21 groups of *in vivo* structural (T2-w) MRI, functional dynamic contrast enhanced (DCE) MRI, and *ex vivo* WMH images with cancer present. Our method determines a non-linear transformation to align WMH with the high resolution *in vivo* T2-w MRI, followed by mapping of the histopathologic cancer extent onto the T2-w MRI. The cancer extent is then mapped from T2-w MRI onto DCE-MRI using the combined non-rigid and affine transformations determined by the registration. Evaluation of prostate registration is performed by comparison with the 3 time point (3TP) representation of functional DCE data, which provides an independent estimate of cancer extent. The set of synthetic multiprotocol images, acquired from the BrainWeb Simulated Brain Database, comprises 11 pairs of T1-w and proton density (PD) MRI of the brain. Following the application of a known warping to misalign the images, non-rigid registration was then performed to recover the original, correct alignment of each image pair. Quantitative evaluation of brain registration was performed by direct comparison of (1) the recovered deformation field to the applied field and (2) the original undeformed and recovered PD MRI. For each of the data sets, COLLINARUS is compared with the MI-driven counterpart of the B-spline technique. In each of the quantitative experiments, registration accuracy was found to be significantly ($p < 0.05$) for COLLINARUS compared with MI-driven B-spline registration. Over 11 slices, the mean absolute error in the deformation field recovered by COLLINARUS was found to be 0.8830 mm.

Keywords: quantitative image analysis, magnetic resonance, whole-mount histology, image registration,prostate, cancer, B-splines, COFEMI, hierarchical, non-rigid

1. INTRODUCTION

Multimodal and multiprotocol image registration refers to the process of alignment of two images obtained from different imaging modalities (e.g. digitized histology and MRI) and protocols (e.g. T2-weighted and PD MRI), utilizing either rigid or non-rigid coordinate system transformations. Both processes are critical components in a range of applications, including image guided surgery,[1–3] multimodal image fusion for cancer diagnosis and treatment planning,[4] and automated tissue annotation.[5] However, registration of multimodal imagery has posed a more challenging task compared with alignment of images from the same modality or protocol

Contact: Anant Madabhushi: E-mail: anantm@rci.rutgers.edu, Telephone: 1 732 445 4500 x6213

Medical Imaging 2009: Image Processing, edited by Josien P. W. Pluim, Benoit M. Dawant,
Proc. of SPIE Vol. 7259, 72592N · © 2009 SPIE
CCC code: 1605-7422/09/$18 · doi: 10.1117/12.812352

on account of differences in both image intensities and shape of the underlying anatomy. The first of these hinderances, dissimilar intensities between modalities, arises as a consequence of the measurement of orthogonal sources of information such as functional (SPECT) and structural (CT/MRI) imagery,[4] as well as on account of other factors such as intensity artifacts, resolution differences, and weak correspondence of observed structural details. We have previously addressed these challenges in the context of rigid registration using our feature-driven registration scheme termed combined feature ensemble mutual information (COFEMI).[6,7] The goal of the COFEMI technique is to provide a similarity measure that is driven by unique low level textural features, for registration that is more robust to intensity artifacts and modality differences than similarity measures restricted to intensities alone. For example, the multiprotocol MRI in Fig. 1 which contains strong bias field artifact on T1 MRI are registered using both conventional intensity-based MI and with COFEMI. The features in Figs. 1(e) and (e) clearly demonstrate robustness to artifacts, and hence provide improved registration with COFEMI as in Fig. 1(f). We refer the reader to [6] for demonstration and further description of the technique.

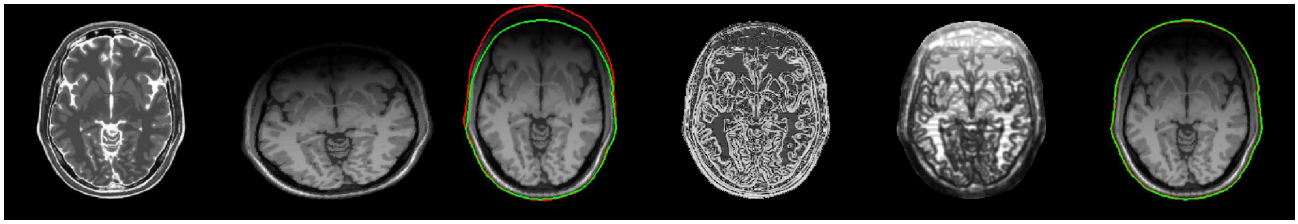

Figure 1. Comparison of MI and feature-driven COFEMI rigid registration of images with strong bias field inhomogeneity artifacts. (a) A T2 MR brain image is registered to (b) the corresponding T1 MRI using (c) intensity-based MI and (f) COFEMI using second order (d) correlation and (e) inverse difference moment features. Green contours in (c) and (f) represent the boundary of the T2 brain MRI of (a) overlaid onto the registered target. Red outlines accentuate the boundaries in the registration result. Use of textural feature images by COFEMI was shown to improve registration of multiprotocol images with heavy intensity artifacts.

While accurate rigid registration is a valuable precursor to more complex transformations, and rigid image transformations are often sufficient to model many deformations in biomedical imagery, non-linear shape differences are common between real multimodal biomedical image data sets. For example, registration of images of highly deformable tissues such as in the breast have been shown to require flexible non-rigid techniques.[8] Similarly, non-linear differences in the overall shape of the prostate between *in vivo* MRI and *ex vivo* whole mount histology (WMH) have been shown to exist as a result of (1) the presence of an endorectal coil during MR imaging and (2) deformations to the histological specimen as a result of fixation and sectioning.[9,10] Consequently, achieving correct alignment of such imagery requires elastic transformations to overcome the non-linear shape differences. The free form deformation (FFD) technique proposed by Rueckert in [8] has been demonstrated to provide a flexible automated framework for non-rigid registration by using any similarity measure to drive registration. However, this technique relies upon intensity-based similarity measures, which have been shown to be wanting for robustness across highly dissimilar modalities and in the presence of artifacts.[6] Thin plate splines (TPS) warping methods are common, but involve identification of anatomical fiducials, a difficult task that is usually performed manually.

To overcome the challenges of both non-linear deformations and intensity artifacts simultaneously, we present a new technique termed Feature Ensemble Multi-level Splines (COLLINARUS). Our new COLLINARUS non-rigid registration scheme offers the robustness of COFEMI to artifacts and modality differences, while allowing fully automated non-linear image warping at multiple scales via a hierarchical B-spline mesh grid optimization scheme. An overview of the registration methodology used in this paper to demonstrate COLLINARUS is presented in Fig. 2, whereby feature ensembles drive both rigid and non-rigid registration of an intensity image that is the target for transformation, onto a template intensity image that remains stationary. As previously described,[6] COFEMI is used to drive an initial rigid registration step to correct large scale translations, rotations, and differences in image scale. The transformed target intensity image that results from rigid registration is then registered in a non-linear fashion via COLLINARUS to the template image. Registration by COLLINARUS is

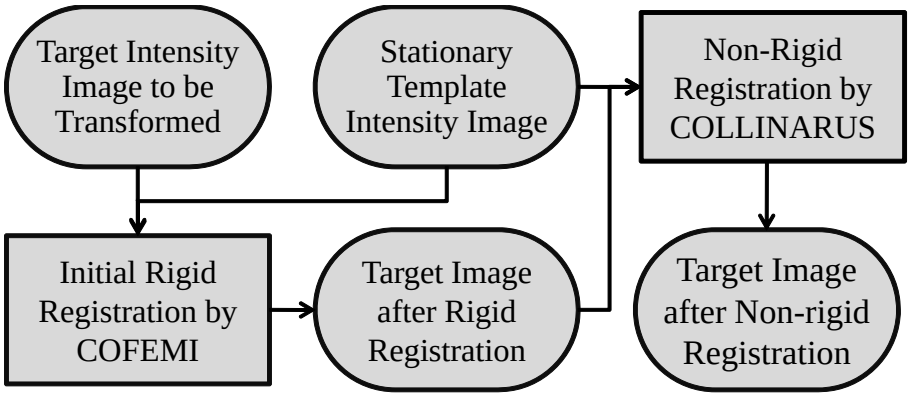

Figure 2. A two step COFEMI-driven rigid and non-rigid registration methodology applied in this study to perform automated alignment of two intensity images. Initial global alignment is performed using COFEMI to optimize an affine transformation of the target intensity image. Subsequently, non-rigid registration via COLLINARUS is performed to determine the remaining local deformations.

critical to account for local deformations that cannot be modeled by any linear coordinate transformation. Since COFEMI and COLLINARUS involve maximization of a similarity measure, each step is fully automated.

We developed the COLLINARUS scheme to perform an automated tissue annotation task that is designed to facilitate the development and evaluation of a novel system for computer-assisted detection (CAD) of prostate cancer on multi-protocol MRI.[11] The development of a multimodal CAD system that operates upon *in vivo* imagery requires ground truth labels for cancer on each modality to characterize malignant tissue. Since these MRI pixel labels are usually obtained by manual delineation of cancer, they can be extremely time consuming to generate and subject to errors and bias of the expert performing the annotation. The deleterious effect of such errors in training labels on MRI CAD has been demonstrated.[12,13] Therefore, to improve labeling and hence CAD classifier accuracy, alignment of *in vivo* imagery with corresponding *ex vivo* whole mount histology (WMH), the source of the cancer "gold standard", may be performed via automated multimodal image registration. The use of COFEMI for automated rigid registration has been previously demonstrated on *ex vivo* MRI.[14] In the current study, we present the non-rigid spatial registration of *in vivo* T2-w MRI, *in vivo* DCE MRI, and *ex vivo* whole mount prostate histology slices, followed by mapping of the "gold standard" from histology onto both MRI protocol images. A diagram of the multimodal prostate registration task performed in this paper is shown in Fig. 3. The *ex vivo* WMH containing the "gold standard" label for cancer shown in Fig. 3(a) is registered to the corresponding *in vivo* T2-w MRI section via the COLLINARUS non-linear registration technique. The transformed WMH section shown in the bottom of Fig. 3(a) contains a cancer map than is then transfered directly onto the T2-w MRI as illustrated at the bottom of Fig. 3(b). The new non-rigid COLLINARUS registration technique will overcome the limitations of rigid deformation models, while providing similar improvements in efficiency and accuracy of cancer delineation on *in vivo* multiprotocol MRI. This will allow the structural appearance and functional properties of cancer to be accurately characterized for the development and evaluation of *in vivo* multiprotocol CAD applications.

Qualitative and quantitative evaluation of the COLLINARUS scheme is performed on a set of real multimodal prostate images and on a set of synthetic multiprotocol brain images. Multimodal prostate image registration is performed as described above for 6 clinical data sets comprising a total of 21 groups of *in vivo* T2-w MRI, DCE-MRI, and *ex vivo* WMH images with cancer present. Evaluation of prostate registration is performed by comparison with 3TP DCE mappings, the industry standard for DCE-MRI analysis, and by measures of prostate region overlap. The set of synthetic multiprotocol images, acquired from the BrainWeb Simulated Brain Database,[15] comprises 11 pairs of T1-w and proton density (PD) MRI of the brain. The synthetic registration task was generated by applying a known non-linear warping to the PD MRI, hence misaligning T1-w MRI from PD MRI. Non-rigid registration was then performed to recover the original, correct alignment of each image pair. Quantitative evaluation of brain registration was performed by direct comparison of (1) the recovered deformation field to the applied field and (2) the original undeformed and recovered PD MRI. For each of the

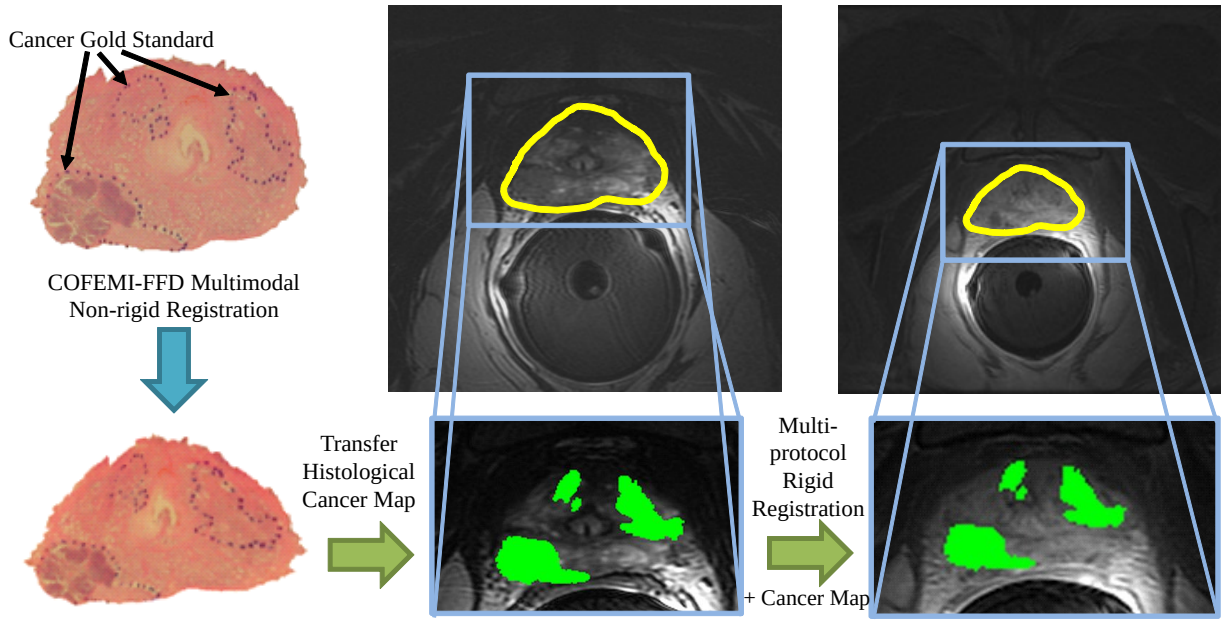

Figure 3. Application of the COLLINARUS automated feature driven non-rigid registration technique to alignment of (a) *ex vivo* whole mount histology (WMH), (b) *in vivo* T2-w MRI and (c) *in vivo* DCE-MRI images of the prostate and annotation of cancer on multiprotocol MRI. (a) Histopathologic staining of whole-mount sections of a prostate with cancer provides the "gold standard" for cancer extent. Non-rigid registration via COLLINARUS of (a) WMH to (b) corresponding *in vivo* MRI obtained prior to resection allows the histological cancer map to be transferred onto (b). (c) Corresponding DCE-MRI is registered to (b) by COFEMI rigid registration to establish a map of cancer on (c).

data sets, COLLINARUS is compared with the MI-driven counterpart of the B-spline technique.

The primary novel contributions of this work are,

- A new method termed COLLINARUS for automated non-rigid image registration.
- Use of textural feature image ensembles in a non-rigid registration technique for robustness to artifacts and modality differences.
- A multimodal rigid and non-rigid registration scheme that provides superior registration accuracy compared to use of MI-driven counterparts.

The rest of the paper is organized as follows. In Section 2, the COLLINARUS registration technique is described. In Section 3, the results of the real and synthetic registration tasks are described for both COLLINARUS and MI-MLS. Concluding remarks are given in Section.[15]

2. COLLECTION OF IMAGE-DERIVED NON-LINEAR ATTRIBUTES FOR REGISTRATION USING SPLINES (COLLINARUS)

2.1 Overview

The new registration technique referred to as Collection of Image-derived Non-linear Attributes for Registration Using Splines, or COLLINARUS, consists of three primary components,

1. A robust feature ensemble-driven similarity measure derived the COFEMI[6] scheme,
2. A flexible non-linear image warping model based on B-splines and,
3. A variable spline grid size approach for optimizing a multi-scale local image warping.

2.2 Notation

Define a stationary template image as $\mathcal{A} = (C, f^A)$, where C is a set of coordinates $c \in C$ and $f^A(c)$ is the intensity value of $\mathcal{A}$ at location c. A target image $\mathcal{B} = (C, f^B)$ is similarly defined with intensities $f^A(c)$ on the same coordinate grid C. The goal of the registration task is to provide a coorinate transformation $\mathbf{T}(c)$, $\forall c \in C$, that describes the mapping of each point on a registered target image $\mathcal{B}^r$ to the template intensity image $\mathcal{A}$. We can then define $\mathcal{B}^r = (C, f^*(c))$, where $f^*(c) = g(\mathbf{T}(c), f^B)$ represents an interpolation function used to provide intensity values at location $\mathbf{T}(c)$ using the underlying intensity map f^B. We can further define a generic image transformation $\mathbf{\Phi}$ to represent the application of $\mathbf{T}$ at each $c \in C$, such that $\mathcal{B}^r = \mathbf{\Phi}(\mathcal{B}, \mathbf{T})$.

2.3 General Registration Framework

We demonstrate COLLINARUS in a two stage rigid and non-rigid registration framework, whereby COFEMI and COLLINARUS are used in the rigid and non-rigid components, respectively. As described in Fig. 2, registration of $\mathcal{A}$ and $\mathcal{B}$ may be performed by first determining a global, rigid transformation $\mathbf{T}_{rigid}$, followed by an local, elastic transformation $\mathbf{T}_{elastic}$. The global transformation is determined by maximizing,

$$\mathbf{T}_{rigid} = \underset{\mathbf{T}}{\operatorname{argmax}}\, \psi(\mathcal{A}, \mathbf{\Phi}(\mathcal{B}, \mathbf{T})), \tag{1}$$

where ψ is an image similarity measure such as conventional intensity-driven MI or the feature ensemble-driven measure from COFEMI. Application of $\mathbf{T}_{rigid}$ to $\mathcal{B}$ gives the rigidly registered target image B^r by,

$$\mathcal{B}^r = \mathbf{\Phi}(\mathcal{B}, \mathbf{T}_{rigid}). \tag{2}$$

The elastic transformation $\mathbf{T}_{elastic}$ and the final registered target image $\mathcal{B}^{nr}$ are then determined, again by maximization of the similarity measure ψ, by,

$$\mathbf{T}_{elastic} = \underset{\mathbf{T}}{\operatorname{argmax}}\, \psi(\mathcal{A}, \mathbf{\Phi}(\mathcal{B}^r, \mathbf{T})), \text{ and} \tag{3}$$

$$\mathcal{B}^{nr} = \mathbf{\Phi}(\mathcal{B}^r, \mathbf{T}_{elastic}). \tag{4}$$

A unified coordinate transformation may then be defined as the successive application of the coordinate transformations $\mathbf{T}_{rigid}$ and $\mathbf{T}_{elastic}$,

$$\mathbf{T}^*(c) \equiv \mathbf{T}_{elastic}(\mathbf{T}_{rigid}(c)) \tag{5}$$

and the non-rigid registration result generated directly by,

$$\mathcal{B}^{nr} = \mathbf{\Phi}(\mathcal{B}, \mathbf{T}^*) \tag{6}$$

For the implementation of the above methodology used in this study, we define $\mathbf{T}_{rigid}$ as an affine coordinate transformation. Details of the multi-scale optimization of $\mathbf{T}_{elastic}$ are described in the following section.

2.4 COLLINARUS Non-Rigid Registration

The COLLINARUS non-rigid registration technique achieves the optimization of $\mathbf{T}_{elastic}$ in Eqn. (3) by synergy of the following concepts,

1. Using a feature ensemble-driven similarity measure for ψ, obtained via the techniques for feature extraction, selection, and combination that are associated with COFEMI.
2. Defining $\mathbf{T}_{elastic}$ as the 2-D tensor product of the cubic B-splines[16,17] to allow local elastic image deformations.
3. Maximization of ψ using a multi-level control point grid approach to achieve B-spline deformations at multiple scales.

The feature ensemble-driven similarity measure used for ψ is obtained by the COFEMI technique. The primary components of COFEMI are (1) extraction of an exhaustive set of low level textural feature images, (2) selection of a highly descriptive ensembles of textural features from the intensity images using the *CMIfeatures* algorithm described in [6], and (3) incorporation of the feature ensembles by combined mutual information (CMI), a form of MI derived to compare two multivariate observations. The measure ψ used by COLLINARUS is thus defined as in [6] by,

$$\psi(\mathcal{A}, \mathcal{B}) = CMI(\mathcal{A}\,\pi^A, \mathcal{B}\,\pi^B), \tag{7}$$

where π^A and π^B are the selected feature ensembles, and each $\mathcal{A}\,\pi^A$ and $\mathcal{B}\,\pi^B$ also represent distinct ensembles. Thus, the COLLINARUS non-rigid registration scheme involves optimization of $\mathbf{T}_{elastic}$ by Eqn. (3) via (7), whereas the COFEMI rigid registration scheme involves optimization of $\mathbf{T}_{rigid}$ by Eqn. (1) via (7).

By defining $\mathbf{T}_{elastic}$ for COLLINARUS in terms of the cubic B-splines basis functions, COLLINARUS is capable of defining local elastic deformations without the use of anatomical fidicual markers. The coordinate transformation used by COLLINARUS is instead defined in terms of a regularly spaced control point mesh of size $n_x \times n_y$, the displacements of which are used to define a coordinate transformation $\mathbf{T}_{elastic}$ according to the 2D tensor product of B-spline basis functions.[17]

The multiresolution image warping method employed by COLLINARUS is achieved by a multi-level spline grid optimization approach, whereby the number of grid points are modulated via n_x and n_y. Spline deformations defined with successively finer control point meshes are then combined into a single non-linear transformation. The idea behind this approach is to exploit the local neighborhood influence of B-splines grid so as to model successively smaller and more local deformations. This technique is thus capable of modeling deformations of varying magnitude. For a total of L transformations, $\mathbf{T}^l_{elastic}$ is defined at multiple control point spacing levels $l \in \{1, \ldots, L\}$ with corresponding mesh sizes $n_{x,l} \times n_{y,l}$. At each level l, the transformation $\mathbf{T}^l_{elastic}$ is determined as in Eqn. 3 by maximization of similarity measure ψ, where the displacements of each of the $n_{x,l} \times n_{y,l}$ control points are the free parameters. Each $\mathbf{T}^l_{elastic}$ is applied successively to form the final elastic transformation $\mathbf{T}_{elastic}$.

2.5 Registration Evaluation

Evaluation of registration accuracy can be performed easily if the correct coordinate transformation, $\mathbf{T}'$, is known. First, the magnitude of error in the transformation $\mathbf{T}^*$ determined by registration can be quantified in terms of mean absolute difference (MAD) ($F_{mad}(\mathbf{T}^*)$) and root mean squared (RMS) error ($F_{rms}(\mathbf{T}^*)$) from $\mathbf{T}'$,

$$F_{mad}(\mathbf{T}^*) = \frac{1}{N} \sum_{c \in C} \mathbf{T}^*(c) - \mathbf{T}'(c) \tag{8}$$

$$F_{rms}(\mathbf{T}^*) = \sqrt{\frac{1}{N} \sum_{c \in C} (\mathbf{T}^*(c) - \mathbf{T}'(c))^2}. \tag{9}$$

Further, the desired transformed target image $\mathcal{B}'$ may be obtained by from the known correct transformation $\mathbf{T}'$ by,

$$\mathcal{B}' = \mathbf{\Phi}(\mathcal{B}, \mathbf{T}'), \tag{10}$$

and compared directly with the resulting target image $\mathcal{B}^{nr}$ actually obtained from registration. Three measures are used to compare $\mathcal{B}^{nr}$ with $\mathcal{B}'$, including L2 distance (D_{L2}), MI (S_{MI}), and entropy correlation coefficient (S_{ECC}).[18]

3. RESULTS

3.1 Data Sets

Synthetic Data. Synthetic brain MRI[15] were obtained from BrainWeb, comprising corresponding simulated T1-w and PD MR brain volumes of dimensions $181 \times 217 \times 181$ with voxel size of 1mm^3. We denote the T1-w and PD MRI images as $\mathcal{C}^{T1}$ and $\mathcal{C}^{PD}$, respectively. Ground truth for correct alignment between $\mathcal{C}^{T1}$ and $\mathcal{C}^{PD}$ is implicit in the simulated data, allowing use of the evaluation methods described in Sec. 2.5.

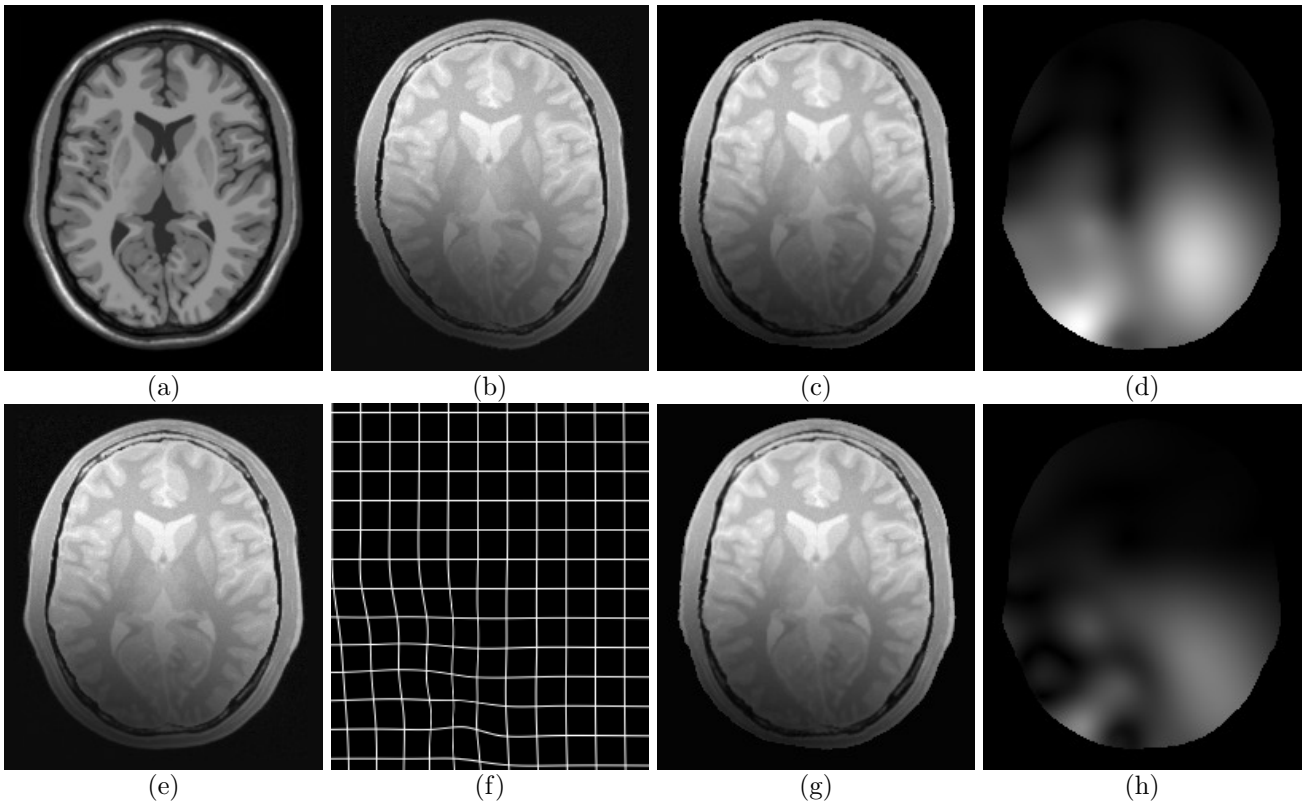

Figure 4. (a) Synthetic T1-w MRI section, and (e) corresponding PD MRI section with simulated noise and bias field inhomogeneity artifacts. A deformation field, demonstrated on a grid in (f), is applied to (e) PD MRI to generate (b) a warped PD MRI section. Both MI and COFEMI are used to drive a non-linear B-spline based registration of (b) to (a). A correctly transformed PD MRI section would closely resemble (f). The results of (e) MI-driven and (g) COLLINARUS registration appear similar, while representations of the deformation field error magnitudes in (d) and (h) illustrate the greater error of MI compared with COFEMI.

Clinical Data. Clinical *in vivo* multiprotocol (T2-w and DCE) 3T MRI images with WMH sections of the prostate were acquired to establish a map for spatial extent of cancer on both T2-w MRI and DCE-MRI. For 6 clinical data sets comprising *in vivo* T2-w MRI, DCE-MRI, and WMH, a total of 21 corresponding images with cancer present were considered. Cancer extent on histology was first obtained via microscopic analysis of hematoxylin and eosin stained tissue. Slices of T2-w MRI that correspond with the available WMH sections were identified by visual inspection by an expert radiologist. The slices of the T2-w MRI and DCE-MRI volumes are in implicit correspondence (but not 2D alignment) since the multiprotocol MRI data was acquired during a single scanning session in which the patient remained stationary.

3.2 Synthetic Brain Data

The synthetic T1-w and PD MRI brain data was used to perform quantitative analysis of registration accuracy under simulated noise and intensity inhomogeneity. Since the $\mathcal{C}^{T1}$ and $\mathcal{C}^{PD}$ images generated by the BrainWeb MRI simulator are in implicit alignment, evaluation of registration accuracy was performed as described in Sec. 2.5 by imposing a known transformation T' to each coordinate of $\mathcal{C}^{PD}$, followed by execution of COLLINARUS to determine the transformation T^* required to recover the original alignment. For 11 pairs of corresponding $\mathcal{C}^{T1}$ and $\mathcal{C}^{PD}$ images, registration was performed using COLLINARUS and an analogous MI-driven B-spline registration scheme. Fig. 4 demonstrates the registration of one T1-w MRI section with a PD MRI section. The T1-w MRI in Fig. 4(a) is initially in alignment with the PD MRI in 4(b), which contains noise and simulated field inhomogeneity. The non-linear deformation illustrated in Fig. 4(c) by the deformed grid is then applied to generate the deformed PD MRI in Fig. 4(d). MI-driven B-spline registration is then performed to obtain

the PD MRI image in Fig. 4(e). A textural feature calculated by COLLINARUS from Fig. 4(b) is shown in Fig. 4(g), demonstrating the diminished effect of inhomogeneity on the feature image. The registration result from COLLINARUS is shown in Fig. 4(h). While the MI-based and COLLINARUS results in Figs. 4(e) and (h) appear similar, deformation field error magnitude images shown in Fig. 4(f) and (i) clearly indicate that $\mathbf{T}^*$ obtained from COLLINARUS contains far less error than the transformation obtained MI spline registration.

The quantities F_{mad} and F_{rms} are calculated from $\mathbf{T}^*$ obtained from COLLINARUS and MI-MLI from Eqns. (9), as well as D_{L2}, S_{MI}, and S_{ECC}. The average values of each quantity for $n = 11$ image pairs are given in Table 1, along with p-values for student's t-tests. The average values of both F_{mad} and F_{rms} were significantly lower for COLLINARUS, indicating less error in the recovered deformation field determined by $\mathbf{T}^*$. The average values of both S_{MI}, and S_{ECC} were significantly higher for COLLINARUS, indicating greater similarity between the recovered PD MRI and the correct undeformed image. Similarly the distance D_{L2} was lower for COLLINARUS, indicating greater similarity between COLLINARUS recovered and correct PD images.

	F_{mad}	F_{rms}	D_{L2}	S_{MI}	S_{ECC}
MI-MLS	0.9585	2.2201	1.88e+03	2.8803	0.5104
COLLINARUS	**0.8330**	**1.9406**	**1.56e+03**	**3.0709**	**0.5437**
p $(n = 11)$	0.0075	0.0097	9.97e-05	8.76e-05	9.97e-05

Table 1. Comparison of non-rigid registration accuracy for COLLINARUS and MI-MLS alignment of $n = 11$ pairs of synthetic PD MRI and T1-w MRI brain images. Error of recovered deformation field in terms of mean absolute difference (F_{mad}) and root mean squares (F_{rms}) measures the deviation of the registration-derived deformation field from the known field. Units of F_{mad} and F_{rms} are mm. Euclidean distance between the original undeformed PD MRI and recovered PD MRI obtained by non-rigid registration (D_{L2}), measures the disimilarity between the registration result and the ideal result. The mutual information and entropy correlation coefficient between the recovered and original PD MRI sections (S_{MI} and S_{ECC}) indicate how well the recovered image resembles the original, ideal result. Each of F_{mad}, F_{rms}, D_{L2}, S_{MI} and S_{ECC} indicate that COLLINARUS more accuratlely recovered the original undeformed PD MRI compared with MI-MLS.

3.3 Clinical Multi-Modal Prostate Data

3.3.1 Prostate Registration Task

The "gold standard" for cancer presence, which is available on the whole mount histological (WMH) images, is mapped onto both *in vivo* T2-w MRI and DCE-MRI by alignment of each of the modalities. In this taks, large differences in the overall shape of the prostate exist between WMH and *in vivo* MRI as a result of (1) the presence of an endorectal coil during MR imaging and (2) deformations to the histological specimen as a result of fixation and sectioning. Consequently, achieving correct alignment of WMH and MRI requires elastic transformations to overcome the non-linear shape differences. Thus, a multi-stage rigid and non-rigid registration procedure utilizing COLLINARUS was implemented to align the WMH, T2-w MRI, and DCE-MRI. The main steps are described below:

1. Initial affine registration of the WMH target image to the *in vivo* T2-w MRI image via the COFEMI multiple feature-driven registration technique.
2. Non-rigid registration of rigidly registered WMH image from step 1 onto T2-w MRI using the COLLINARUS technique.
3. Combine the resulting affine and non-rigid transformations, mapping pixels from WMH onto the T2-w MRI.
4. Affine registration of multiprotocol images (T2-w MRI and DCE) via maximization of mutual information (MI), bringing all modalities and protocols in to spatial alignment.

In step 2, the B-spline derived warping from COLLINARUS allows for modeling of the local deformations that result from the presence of the endorectal coil required for high resolution *in vivo* MRI of the prostate. On the other hand, since T2-w MRI and DCE-MRI were acquired during the same scanning session, only a rigid

transformation was required in step 4 to compensate for resolution and bounding box differences, as well as any small patient movements that may have occurred between acquisition of the two protocol volumes. The combined non-linear transformation obtained in step 3 was applied to the histopathologic cancer label, hence bringing the label into the coordinate frame of T2-w MRI. The final determined affine transformation was then applied to the histopathologic cancer label on T2-w MRI, thus generating the label for cancer extent on DCE-MRI.

3.3.2 Three Time Point (3TP) DCE Cancer Maps

The commonly used 3 time point (3TP) representation of the DCE-MRI can provide an independent estimate of cancer extent against which the registration-established cancer masks are compared. Most current efforts in computer-aided diagnosis of CaP from DCE-MRI involve pharmacokinetic curve fitting such as in the 3 Time Point (3TP) scheme.[19] Based on the curve/model fits these schemes attempt to identify wash-in and wash-out points, i.e. time points at which the lesion begins to take up and flush out the contrast agent. Lesions are then identified as benign, malignant or indeterminate based on the rate of the contrast agent uptake and wash out. Red, blue and green colors are used to represent different classes based on the ratio $w = \frac{\text{Rate of wash-in}}{\text{Rate of wash-out}}$ of the contrast agent uptake. When w is close to 1, the corresponding pixel is identified as cancerous area (red), when w is close to zero, the pixel is identified as benign (blue), and green pixels are those are identified as indeterminate.

3.3.3 Prostate Registration Results

Corresponding sections from a WMH slice, *in vivo* T2-w MRI, and a single time frame of DCE-MRI imagery from the same patient are shown in Figures 5(a) and (b) for a prostate with cancer, where the boundary of the prostate on T2-w MRI has been outlined in yellow. Using the automated non-rigid registration method described above, the WMH section in Fig. 5(a) is warped into alignment with the prostate region in Fig. 5(b). The cancer extent is then mapped directly onto T2-w MRI, as shown in Figure 5(d) to display the prostate more clearly. Having established cancer extent on T2-w MRI (Fig. 5(d)), the T2-w MRI image is registered to the DCE-MRI image. Finally, the CaP extent is mapped from T2-w MRI (Fig. 5(d)) onto DCE-MRI, as in Figure 5(e). For visual comparison, we calculate the 3TP color representation from the DCE time series, as shown in Fig. 5(f) for the same slice, providing an independent means of evaluating the CaP labels mapped by our registration technique. Prostate overlap between modalities and protocols, and comparison of mapped cancer extent (green) with 3TP cancer extent (red) indicates excellent overall alignment between modalities and protocols obtained by COLLINARUS, and an accurate mapping of cancer on images from both MRI protocols.

Since the correct transformation required to bring the images into alignment is not know, registration accuracy is evaluated in terms of how well the region of the images representing the prostate overlaps between the aligned images (the overlap ratio). The intuition of this measure is that if the prostate image regions completely overlap between the modalities, the registration and hence the cancer mapping is highly accurate. The overlap ratio for two images of the prostate is defined as the ratio of the number of pixel coordinates that represent the prostate in both modalities to the total number of pixel coordinates representing the prostate in either modality (i.e. the prostate region intersection-to-union pixel count ratio). The mean overlap ratio for the prostate in the pairs of registered WMH and T2-w MRI was 0.9261, indicating that prostate in the two aligned modalities occupies nearly the same spatial coordinates. Similarly for the pairs of registered T2-w MRI and DCE-MRI images, a high overlap ratio of 0.8964 was achieved.

4. CONCLUDING REMARKS

We have demonstrated a new method for fully automatic non-rigid multimodal/multiprotocol image registration that combines textural feature ensembles in a similarity measure to drive a multilevel B-spline based image warping scheme. The robustness to modality differences offered by the COFEMI technique for feature ensemble selection and combination, and the flexibility of B-splines to model non-linear deformations are leveraged in this study to provide a powerful tool for automated multimodal image registration. Our method was used to successfully register a unique data set comprising WMH, in vivo T2-w MRI, and in vivo DCE-MRI images of the prostate, and subsequently map histopathologic CaP extent onto the images from both in vivo MRI protocols. A comparison of the CaP labels mapped onto DCE-MRI with the independent 3TP representation suggests that the labels are established accurately by the registration procedure. We have thus presented a robust, accurate

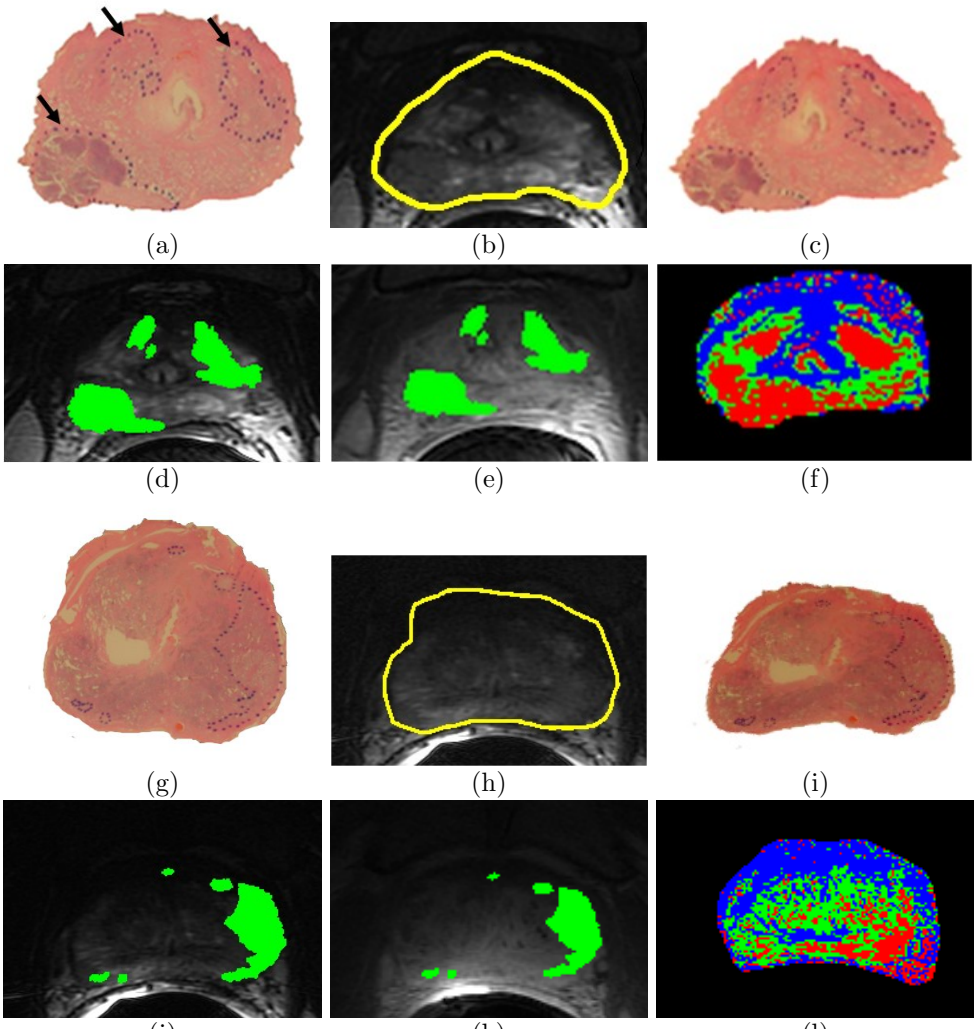

Figure 5. Registration of WMH to 3T in vivo T2-w MRI and DCE-MRI of the prostate with cancer. (a) WMH with cancer extent delineated (dotted lines) is registered to (b) corresponding T2-w MRI using COLLINARUS to generate (c) transformed WMH in spatial alignment with the prostate in (b). (d) T2-w MRI with the cancer extent mapped from (c) superimposed in green. (e) DCE-MRI registered with (d) by an affine transformation, shown with cancer extent (green) mapped from (d) T2-w MRI. (g) The commonly used 3TP representation of the DCE data in (e), which provides and independent estimate of CaP extent, demonstrates that the cancer extent mapped by registration is accurate. (g)-(l) Similar results are demonstrated for a different set of multimodal prostate images from another study.

means for aligning and thus facilitating fusion of structural and functional data. The primary contributions of our method are, The primary novel contributions of this work are,

- A new method termed COLLINARUS that provides flexible and robust automated non-rigid multimodal image registration.
- Use of textural feature image ensembles to drive a non-rigid registration technique and provide robustness to artifacts and modality differences.
- Superior non-rigid registration accuracy compared with similar MI-driven techniques.
- Application of our technique in automatically determining the spatial extent of CaP by registration of multiprotocol 3T in vivo clinical MRI images of the prostate, with histology containing cancer ground

truth. Our work presented here represents the first time a fully automated technique has been presented for registration of histology with *in vivo* MRI of the prostate.

Our experiments on demonstrated on clinical and synthetic data indicated that COLLINARUS provides greater registration accuracy compared with similary MI-driven techniques. As such, the COLLINARUS technique will have broad applicability for automated registration of multimodal and multiprotocol images, including structural and functional data.

ACKNOWLEDGMENTS

This work was funded by: Department of Defense Prostate Cancer Research Program (W81XWH-08-1-0072), The Wallace H. Coulter Foundation (WHCF4-29349, WHCF 4-29368), Busch Biomedical Award, Cancer Institute of New Jersey, New Jersey Commission on Cancer Research, National Cancer Institute (R21-CA127186-01, R03-CA128081-01), Society for Imaging Informatics in Medicine, Rutgers OCLTT Life Science Commercialization Award.

REFERENCES

[1] Fei, B., Wheaton, A., Lee, Z., Duerk, J. L., and Wilson, D. L., "Automatic mr volume registration and its evaluation for the pelvis and prostate.," *Phys Med Biol* **47**, 823–838 (Mar 2002).

[2] Porter, B. et al., "Histology and ultrasound fusion of excised prostate tissue using surface registration," in [*IEEE Ultrasonics Symposium 2001*], 1473–1476 (2001).

[3] Bharatha, A., Hirose, M., et al., "Evaluation of three-dimensional finite element-based deformable registration of pre- and intraoperative prostate imaging," *Medical Physics* **28**(12), 2551–2560 (2001).

[4] Lee, Z., Sodee, D. B., Resnick, M., and Maclennan, G. T., "Multimodal and three-dimensional imaging of prostate cancer.," *Comput Med Imaging Graph* **29**, 477–486 (Sep 2005).

[5] Mansoori, T., Plank, G., Burton, R., Schneider, J., Kohl, P., Gavaghan, D., and Grau, V., "An iterative method for registration of high-resolution cardiac histoanatomical and mri images.," in [*IEEE Proc. ISBI*], 572–575 (2007).

[6] Chappelow, J., Madabhushi, A., et al., "A combined feature ensemble based mutual information scheme for robust inter-modal, inter-protocol image registration," in [*International Symposium on Biomedical Imaging*], IEEE (2007).

[7] Chappelow, J., Madabhushi, A., Rosen, M., Tomaszeweski, J., and Feldman, M., "A combined feature ensemble based mutual information scheme for robust inter-modal, inter-protocol image registration," in [*Biomedical Imaging: From Nano to Macro, 2007. ISBI 2007. 4th IEEE International Symposium on*], 644–647 (12-15 April 2007).

[8] Rueckert, D., Sonoda, L. I., Hayes, C., Hill, D. L., Leach, M. O., and Hawkes, D. J., "Nonrigid registration using free-form deformations: application to breast mr images.," *IEEE Trans. Med. Imag.* **18**, 712–721 (Aug 1999).

[9] Hensel, J. M., Mnard, C., Chung, P. W., Milosevic, M. F., Kirilova, A., Moseley, J. L., Haider, M. A., and Brock, K. K., "Development of multiorgan finite element-based prostate deformation model enabling registration of endorectal coil magnetic resonance imaging for radiotherapy planning," *International Journal of Radiation Oncology•Biology•Physics* **68**(5), 1522 – 1528 (2007).

[10] Taylor, L. S., Porter, B. C., Nadasdy, G., di Sant'Agnese, P. A., Pasternack, D., Wu, Z., Baggs, R. B., Rubens, D. J., and Parker, K. J., "Three-dimensional registration of prostate images from histology and ultrasound.," *Ultrasound Med Biol* **30**, 161–168 (Feb 2004).

[11] Madabhushi, A., Feldman, M. D., et al., "Automated detection of prostatic adenocarcinoma from high-resolution *ex vivo* MRI," *IEEE Trans. Med. Imag.* **24**, 1611–1625 (December 2005).

[12] Madabhushi, A., Shi, J., et al., "Graph embedding to improve supervised classification and novel class detection: application to prostate cancer," in [*Medical Image Computing and Computer-Assisted Intervention 2005*], Duncan, J. S. and Gerig, G., eds., 729–737 (2005).

[13] Muhlenbach, F., Lallich, S., and Zighed, D. A., "Identifying and handling mislabelled instances," *J. Intell. Inf. Syst.* **22**(1), 89–109 (2004).

[14] Chappelow, J., Viswanath, S., Monaco, J., Rosen, M., Tomaszewski, J., Feldman, M., and Madabhushi, A., "Improving supervised classification accuracy using non-rigid multimodal image registration: detecting prostate cancer," in [*Medical Imaging 2008: Computer-Aided Diagnosis. Edited by Giger, Maryellen L.; Karssemeijer, Nico. Proceedings of the SPIE, Volume 6915, pp. 69150V-69150V-12 (2008).*], *Presented at the Society of Photo-Optical Instrumentation Engineers (SPIE) Conference* **6915** (Apr. 2008).

[15] Collins, D. L., Zijdenbos, A. P., Kollokian, V., Sled, J. G., Kabani, N. J., Holmes, C. J., and Evans, A. C., "Design and construction of a realistic digital brain phantom.," *IEEE Trans. Med. Imag.* **17**, 463–468 (Jun 1998).

[16] Lee, S., Wolberg, G., Chwa, K.-Y., and Shin, S. Y., "Image metamorphosis with scattered feature constraints," *IEEE Trans. Vis. Comput. Graphics* **2**, 337–354 (Dec. 1996).

[17] Lee, S., Wolberg, G., and Shin, S. Y., "Scattered data interpolation with multilevel b-splines," *IEEE Trans. Vis. Comput. Graphics* **3**, 228–244 (July–Sept. 1997).

[18] Maes, F., Collignon, A., Vandermeulen, D., Marchal, G., and Suetens, P., "Multimodality image registration by maximization of mutual information.," *IEEE Trans. Med. Imag.* **16**, 187–198 (Apr 1997).

[19] Degani, H., Gusis, V., et al., "Mapping pathophysiological features of breast tumours by MRI at high spatial resolution," *Nature Medicine* **3(7)**, 780–782 (1997).